PCCP

Accepted Manuscript

ROYAL SOCIETY OF CHEMISTRY

www.rsc.org/pccp

Journal Name

RSCPublishing

ARTICLE

Physical properties of high Li-ion content *N*-propyl-*N*-methylpyrrolidinium bis(fluorosulfonyl)imide based ionic liquid electrolytes

Cite this: DOI: 10.1039/x0xx00000x

Received 00th January 2012,
Accepted 00th January 2012

DOI: 10.1039/x0xx00000x

www.rsc.org/

Hyungook Yoon[a], Adam S. Best[b], Maria Forsyth[a], Douglas R. MacFarlane[c], and Patrick C. Howlett[a]

Electrolytes based on bis(fluorosulfonyl)imide (FSI) with a range of LiFSI salt concentrations were characterized using physical property measurements, as well as NMR, FT-IR and Raman spectroscopy. Different from the behavior at lower concentrations, the FSI electrolyte containing 1:1 salt to IL mole ratio) showed less deviation from the KCl line in the Walden plot, suggesting greater ionic dissociation. Diffusion measurements show higher mobility of lithium ions compared to the other ions, which suggests that the partial conductivity of Li^+ is higher at this higher composition. Changes in the FT-IR and Raman peaks indicate that the cis-FSI conformation is preferred with increasing Li salt concentration.

Introduction

Because of their negligible vapor pressure and wide electrochemical windows, ionic liquids (ILs) have been considered viable replacements for current organic-liquid based electrolytes for lithium batteries.[1] Of the various ILs studied, those which include the bis(fluorosulfonyl)imide (FSI) anion have gained significant attention for their relatively low viscosity and high conductivity.[2] This anion was first introduced by Armand et al.,[3] and organic liquids containing lithium FSI were successfully used as lithium battery electrolytes by Zaghib et al.[4]. Matsumoto et al.[2] reported that FSI based ILs show fast charging ability with $LiCoO_2$ cathodes, and Ishikawa et al.[5] demonstrated stable cycling ability with graphite anodes, with no organic diluents or additives.[5] There have also been many subsequent studies applying this FSI based electrolyte in lithium batteries.[6-13] Some drawbacks of this IL have also been reported, including concerns about high temperature stability and its corrosive properties.[14-16]

To understand the superior qualities of FSI based ILs - in particular low viscosity and high conductivity, there have been many investigations of their physicochemical and electrochemical properties, including comparative studies with ILs based on the similar bis(trifluoromethylsulfonyl)imide (TFSI) anion. Zhou et al. and Paillard et al. investigated the electrochemical and physicochemical properties of FSI based ILs and their solutions containing Li salts, and demonstrated their superiority compared to the respective TFSI counterparts.[9, 10]

One interesting aspect of this anion is its conformational equilibrium, and since the conformational structure of FSI is similar to that of TFSI, most of this research was originally performed on TFSI, and subsequently similar approaches were taken to see if FSI showed different behavior. For example, Johansson et al. estimated, using ab-initio theoretical calculations, that the TFSI anion can adopt 2 different conformers in liquids.[17] Fujii et al. confirmed, using Raman spectroscopy and molecular dynamics (MD), that TFSI has 2 conformers: C1 (cis-) and C2 (trans-) which are in equilibrium in the liquid state.[18] They then showed that the C1(cis-) form is dominant at higher temperatures, and claimed that the low melting point of TFSI based ILs is related to this behavior.[18] Umebayashi et al. extended this research to ILs containing Li salts, and showed that TFSI ILs prefer cis- conformations and coordinate Li^+ to form $Li(TFSI)_2^-$ or $LiC_2mimTFSI^+$ (1-ethyl-3-methylimidazolium TFSI). In $Li(TFSI)_2^-$, the Li^+ coordinates with 4 oxygen atoms in 2 TFSI anions.[19] Shirai et al. also studied the effects of LiTFSI salt concentration on speciation and coordination in *N*,*N*-diethyl-*N*-methyl-*N*-(2-methoxyethyl) ammonium TFSI by investigating the Raman and NMR shifts.[20] In their study, Li coordinates with 4 oxygen atoms within 2 TFSI anions to form $Li(TFSI)_2^-$ at low Li salt concentration, but forms a lithium oligomer at high Li concentrations.[20] In addition, Ishiguro et al. studied the temperature dependence of the speciation in a highly concentrated LiTFSI (0.171 mol fraction) in C_2mimTFSI solution, and showed that the cis-form of TFSI is more stable than the trans-form at high lithium salt concentration.[21] This research group also compared the coordination behavior of other metal ions such as Li^+, Na^+, K^+ and Cs^+ in solution of their TFSI salts in C_2mimTFSI.[22]

After Beran et al.'s report on the cis- form of the FSI anion in LiFSI salts, showing coordination of Li^+ and oxygen atoms in the FSI anion resulting in clustering around Li^+,[23] Fujii et al. extended their TFSI research to FSI, and demonstrated that FSI also behaves similarly to TFSI. FSI shows cis- and trans-

equilibrium in the liquid state, and the low viscosity of FSI is also related to this conformational equilibrium.[24, 25] The same conclusion was also reached separately by Lopes et al., based on Raman spectroscopy and MD calculations.[26] Recently, some interesting findings were reported by Huang et al., who noted from DSC studies that an exothermic reaction occurs when LiFSI is added into an FSI based IL, Raman spectroscopy was used to show that the Li cation is strongly associated with the FSI anion.[27]

Recently, we have shown that solutions containing a high Li salt concentration, up to 0.5 mol fraction (3.2 mol.kg^{-1}), in an FSI electrolyte can successfully cycle Li | $LiCoO_2$ cells, with fast charging and discharging rate capability (up to 5 C rate at 25 °C), in spite of the high viscosity and relatively low conductivity of these solutions.[28] This suggests that the Li transport mechanism at high lithium salt concentration (> 1.6 mol.kg^{-1}) is different from that at lower lithium concentration (< 1.6 mol.kg^{-1}).[28] In this present study, we now probe the intermolecular interactions to understand why this behavior occurs. We look at physical property changes across a range of Li salt concentrations in C_3mpyr FSI electrolyte, and use ionic conductivity, DSC, FT-IR, Raman and diffusion NMR measurements to elucidate the conduction mechanisms in these electrolytes.

Experimental

Materials:

N-propyl-*N*-methylpyrrolidinium bis(fluorosulfonyl)imide (C_3mpyrFSI, purity > 99.9%) and lithium bis(fluorosulfonyl)imide (LiFSI, purity > 99.5%) were both sourced from Suzhou Fluolyte Co., Ltd., China. Lithium metal was sourced from China Energy Lithium Co., Ltd. (purity > 99.9%).

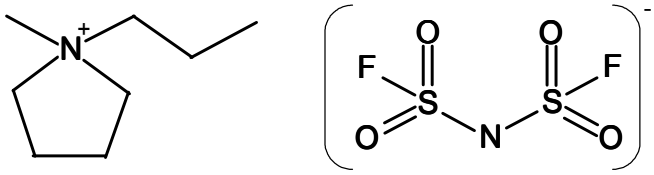

Figure 1 The structure of the ionic liquid in this research, *N*-propyl-*N*-methylpyrrolidinium (C_3mpyr) bis(fluorosulfonyl)imide (FSI)

Electrolytes in this work were prepared by adding LiFSI salts into C_3mpyrFSI IL and stirring for 24 hours at room temperature in an Ar-filled glove box. Moisture contents (< 20 ppm) and halides (Cl < 1 ppm) of all electrolytes were determined via Karl Fisher titrations (Metrohm) and ICP measurements, respectively. Table 1 lists the concentrations of each electrolyte and the molar ratio of each ion in solution. The highest Li salt concentration in this experiment was 3.2 mol.kg^{-1}, which has one Li^+ and one C_3mpyr for every two FSI ions in the solution (i.e., 0.5 mol fraction).

Table 1 Composition of electrolytes investigated.

LiFSI conc. (mol.kg^{-1})	Molar ratio of each ion			FSI : Li
	Li^+	C_3mpyr	FSI	
0 (neat IL)	0	0.50	0.50	
0.4	0.06	0.44	0.50	8.3
0.8	0.10	0.40	0.50	5
1.2	0.14	0.36	0.50	3.6
1.6	0.17	0.33	0.50	2.9
2.0	0.19	0.31	0.50	2.6
2.4	0.21	0.29	0.50	2.4
2.8	0.23	0.27	0.50	2.2
3.2	0.25	0.25	0.50	2

Conductivity, DSC, Viscosity and Density:

To measure ionic conductivity, samples were placed in a sealed glass conductivity dip-cell equipped with two porous platinum electrodes; all preparations took place inside an Ar- filled glove box. 0.01 M KCl solution was used to determine the cell constant, before and after each sample measurement. The ionic conductivity was measured from -50 to 100 °C (with 10 minutes stabilization time after the sample reach the target temperature) and then back to 30 °C to check if there was any hysteresis.
Differential scanning calorimetry (DSC) was carried out on a TA instruments™ DSC 2910. Samples (~10 mg) were sealed in Al hermetic pans (part numbers 900793.901, 900794.901) and then were cooled by liquid nitrogen at 10-20 °C.min^{-1} to -150 °C. The DSC traces were recorded during heating at 10 °C.min^{-1} to 100 °C.

An Anton Paar™ Automated Micro Viscometer with VisioLab ver. 1.0.1 was used to measure viscosity from 25 to 60 °C. An Anton Paar™ DMA 4500M was used to measure density over the same temperature range.

FT-IR:

A Perkin Elmer™ Spectrum 400 FT-IR/FT-NIR Spectrometer with Spectrum ver. 6.3.4 software was used to record FT-IR spectra. A diamond crystal ATR was used at ambient temperature using a sealed ATR cell with a KBr window under argon. The spectrum was accumulated 32 scans from 4000 cm^{-1} to 450 cm^{-1} with 1 cm^{-1} resolution.

Raman:

A Perkin Elmer™ Ramanstation 400F with Spectrum ver. 10.03.06.0100 was used to measure Raman spectra. All spectra were measured at ambient temperature in a glass sample vial from 1600 cm^{-1} to 200 cm^{-1} range with 4 cm^{-1} resolution and 16 scans. The acquired spectrum was subtracted with a spectrum acquired from an empty glass vial. Baseline correction (linear at the two end) and normalization to the highest peak or area were applied to the spectra.

Diffusion NMR:

Pulse-field gradient stimulated echo (PFG-STE) diffusion measurements were performed on a Bruker 300 MHz Ultrashield with Avance I console utilizing a Diff30 diffusion probe and GREAT60 amplifier, following the method described by Bayley et al.[29] The diffusivities of ^{1}H and ^{19}F nuclei were measured for the C_3mpyr cation and FSI anion. ^{7}Li spectra and diffusivities were also measured; the chemical shifts are reported relative to a 2 M LiCl solution. Each sample was packed to a height of 50mm in a 5mm Schott E NMR tube in an Ar filled glove box and sealed with Teflon tape and a cap. Each sample was measured from 278 – 333 K.

Results and Discussion

Conductivity and DSC:

Figure 2(a) shows the ionic conductivity data of LiFSI in C_3mpyrFSI at concentrations from the neat IL to 3.2 mol.kg^{-1}. The ionic conductivity values of the neat C_3mpyrFSI were 5.6 mS.cm^{-1}, 6.5 mS.cm^{-1}, and 7.4 mS.cm^{-1} at 20, 25 and 30 °C respectively, which is lower than the values reported by previous researchers,[2, 5, 6, 8, 14, 30, 31] but closer to more recently reported data.[32] We assume this difference arises from variations in the purity of the neat IL.

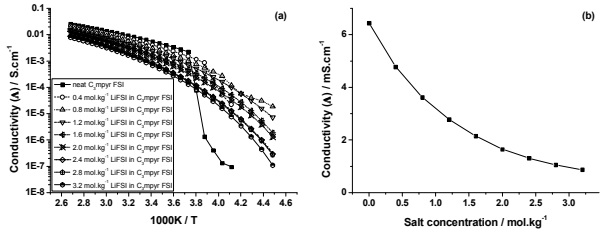

Figure 2 (a) Temperature dependence of ionic conductivity of C_3mpyrFSI with different LiFSI concentrations, (b) Dependence of ionic conductivity on LiFSI concentration in C_3mpyrFSI at 25 °C

The neat IL changes into a solid or plastic crystal phase between -5 and -10 °C with a huge decrease in ionic conductivity. This phase transition shifts to more negative temperatures with increased salt concentration: it is between -15 and -20 °C for 0.4 mol.kg^{-1} solution and between -25 and -30 °C for 0.8 mol.kg^{-1} solution. This phase transition was not observed down to -50 °C when the salt concentration was 1.2 mol.kg^{-1} or greater. We note that the ionic conductivity of the 0.8 mol.kg^{-1} sample in the solid phase below -30 °C is higher than that of 0.4 mol.kg^{-1} in the solid phase or those for the electrolytes of higher salt concentrations (in their liquid state) at the same temperature. The ionic conductivity of the electrolytes in the solid phase has an optimum point, whilst in the liquid phase, conductivity appears to decrease as the salt concentration increases. A similar trend was also observed by Paillard et al. for LiFSI –C_4mpyrFSI electrolyte.[10] This suggests that the ionic conduction mechanism in the solid phase of the FSI electrolyte is quite different to that in the liquid phase. Figure 2(b) demonstrates the concentration dependence of ionic conductivity in C_3mpyrFSI electrolytes, from neat IL through to 3.2 mol.kg^{-1} at 25 °C, showing that the conductivity continuously decreases with increasing salt concentration in the liquid phase.

DSC heating traces from -120 to 100 °C are presented in figure 3 (a) and (b). There are several endothermic transitions in neat C_3mpyrFSI (fig 3(a) bottom curve), including a low energy solid-solid phase transition (phase III – II) with a peak at -78 °C, a combined endothermic-exothermic peak at -46 °C which was described as a mesostable phase transition by Zhou et al.,[9] a solid-solid phase transition (phase II-I) at -16 °C and a melting transition (phase I-liquid) at -6 °C. This DSC result is exactly the same as that reported previously by Zhou et al.,[9] and similar to those reported by Huang et al.[27], and Kunz et al.,[33, 34] except for small peak temperature differences which are probably because of the different scan rate. When Li salt was added to C_3mpyrFSI to make a 0.4 mol.kg^{-1} solution, the melting point decreased to -15 °C, which correlates with the previous conductivity data. An exothermic crystallization peak was observed at -60 °C, and a glass transition at -95 °C. The glass transition temperature moved from -95 °C to -72 °C with the introduction of the lithium salt. The crystallization peak was not observed when the LiFSI salt concentration was 0.2 or 0.3 mol.kg^{-1} (not shown), but was observed when it was 0.5 mol.kg^{-1} or higher (figure 3 (b)). Huang et al has also described similar behaviour in solutions of LiTFSI in C_3mpyrFSI or C_3mpyrTFSI.[27] However, Paillard et al.[10] did not observe this peak for solutions of LiFSI (from 0 to 2.06 mol.kg^{-1}) in C_4mpyr FSI (which has one more methyl group in the chain attached to the pyrrolidinium ring). Instead they found that the IL solutions remained amorphous from neat IL up to a molar ratio of LiFSI : C_4mpyr FSI of 0.4 : 0.6. This may be caused by different thermal histories during the DSC experiments or may suggest that crystal formation in this FSI electrolyte system more readily occurs with the smaller C_3mpyr cation.

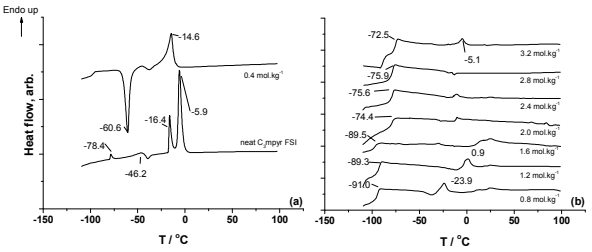

Figure 3 DSC traces for C_3mpyrFSI with LiFSI ionic liquids as a function of LiFSI concentration. a) neat C_3mpyrFSI and 0.4 mol.kg^{-1} LiFSI added, b) 0.8 to 3.2 mol.kg^{-1} LiFSI added. The numbers provided indicate the temperatures of the peak positions.

At higher concentrations, we do note that there is evidence, in some cases, that multiple steps exist in the Tg shown in figure 3 (b). This may not be unexpected due to the high salt concentrations used here; while they are clearly miscible at room temperature there appears to be a phase separation in the glassy state as shown by the steps in Tg.

Density, Viscosity and Walden plots:

A Walden plot based on the Walden equation (eq. 1) described by Angell and co-workers is an effective qualitative method to characterise the properties of an IL.[35]

$$\Lambda\eta^{\alpha} = {}'C \qquad , \qquad (1)$$

where Λ is the molar conductivity, η is the viscosity, α is an adjustable parameter and C is a temperature dependent constant.

The Walden plots of each concentrated electrolyte are shown in figure 4. The slopes of the plots are from 0.9 to 0.95, which is similar to the values generally observed for other ILs.[35-39] The C' values, which represent the distance from the "ideal" aqueous

KCl line, change from -0.009 to -0.446 when going from the neat IL to 2.4 mol.kg^{-1} LIFSI. The trend then changes direction; at 3.2 mol.kg^{-1} LiFSI, $C' = -0.355$. High ionicity is usually indicated by data that lies close to the aqueous KCl line ($\alpha = 1$, $C' = 0$) in the Walden plot;[35, 40] lines far from the ideal line ($C' << 0$) mean that more ions are associated in various forms.[41] Hence, the conductivity did not decrease as much as the viscosity increased when the salt concentration increased from 2.4 mol.kg^{-1} to 3.2 mol.kg^{-1}, which again implies that there may be a different conduction mechanism in the solution with the highest lithium concentration; this mechanism may be related to Li coordination with surrounding ions.

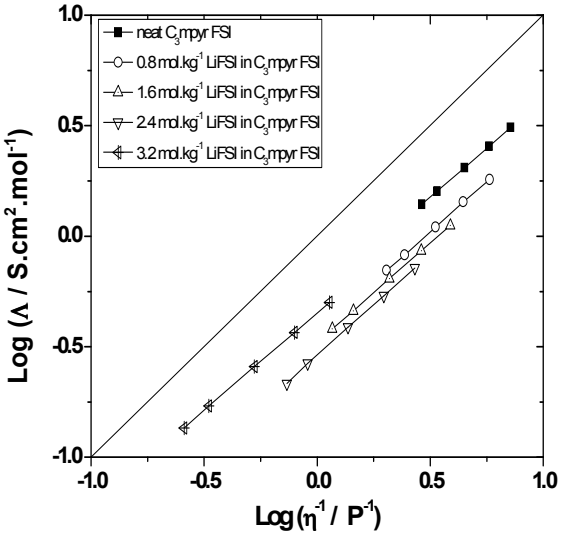

Figure 4 Walden plots showing relationships between inverse viscosity and molar conductivity for C_3mpyrFSI with different LiFSI concentrations and the neat IL

Diffusivity and Ionicity:

To understand the local environment surrounding Li^+ and its effects on ionic mobility and conductivity, 1D NMR spectra and PFG-STE NMR diffusion coefficients for ^{7}Li, ^{1}H, and ^{19}F were measured.

In order to set the pulse sequence for the PFG-STE experiment, we have measured the 1D NMR spectra, Figure 5, which shows that the ^{7}Li NMR peak position unexpectedly shifts to more negative values with increasing Li salt concentration in the electrolytes. This suggests that, as the number of Li^+ ions in the ionic liquid increases, its nearest neighbour environment (and possibly its coordination) changes, resulting in the observed chemical shift. We did not observer similar shifts in either the ^{19}F and ^{1}H spectra under the same experimental conditions, thereby allowing us to rule out magnetic susceptibility effects for the shift in the ^{7}Li spectra.[42] This is somewhat in contrast to work by Shirai et al. in their studies on the effect of LiTFSI concentration in *N*,*N*-diethyl-*N*-methyl-*N*-(2-methoxyethyl) ammonium TFSI; they observed a ^{19}F NMR peak shift to higher ppm, whilst the ^{7}Li peak did not move.[20] With the support of Raman data, they concluded that Li forms $Li(TFSI)_2^-$ in lower concentration solutions and forms a Li oligomer (as also observed in Li_2emim(TFSI)$_3$ ILs by Matsumoto et al.[43]) at higher salt concentrations. Given that our results for the FSI electrolytes presented here are the opposite of those found for the TFSI system, this suggests, somewhat surprisingly, that the coordination of Li in the FSI based ILs is likely to be different.

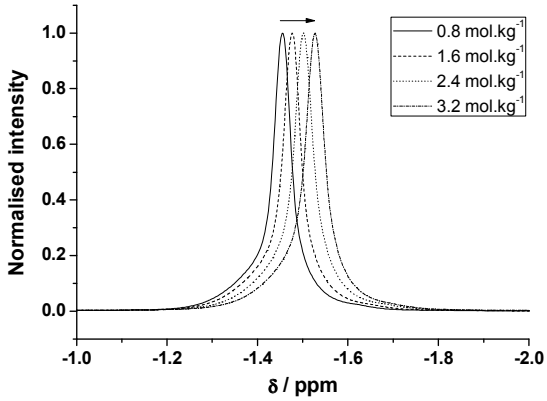

Figure 5 ^{7}Li NMR chemical shifts at 25 °C (2 M LiCl reference). Arrow indicates direction of increasing LiFSI concentration.

The diffusivities of each ion in both the neat IL and the LiFSI solutions, as measured by PFG-STE NMR, are presented in figure 6. The diffusivities of all ions decreased as the Li^+ concentration in solution increased. Figure 6(a) shows the diffusivity plots for neat C_3mpyrFSI, where FSI is faster than C_3mpyr at 25 °C. The difference in diffusivity between the two ions became smaller at 60 °C. When 0.8 mol.kg^{-1} of LiFSI salt was added into the neat IL (figure 6(b) and table 2), the order of diffusivities of the ions at 25 °C was FSI > C_3mpyr > Li^+. As Li salt concentration is further increased up to 3.2 mol.kg^{-1}, the diffusivities of all ion species are decreased. Presumably the addition of Li^+ decreases the fluidity of the entire system and hence all ions show a decreased diffusivity, however, as seen from figure S1, the rate at which the diffusion coefficient decreases with increasing LiFSI concentration is greatest for the FSI ion, followed by C_3mpyr and finally the Li^+ diffusivity. Since a high Li^+ concentration means a relatively smaller amount of C_3mpyr interacting with the FSI, this trends implies that the Li^+ ion has a much stronger influence on the FSI diffusion and thus possibly implies a more aggregated structure whereby the ions are not moving independently of one another but rather as a larger species. Interestingly, for all concentrations, the temperature dependence of the diffusion coefficients for both cations is almost identical, indicating similar activation energies, whereas the anion appears to have an apparently smaller activation energy for all compositions, even in the neat ionic liquid.

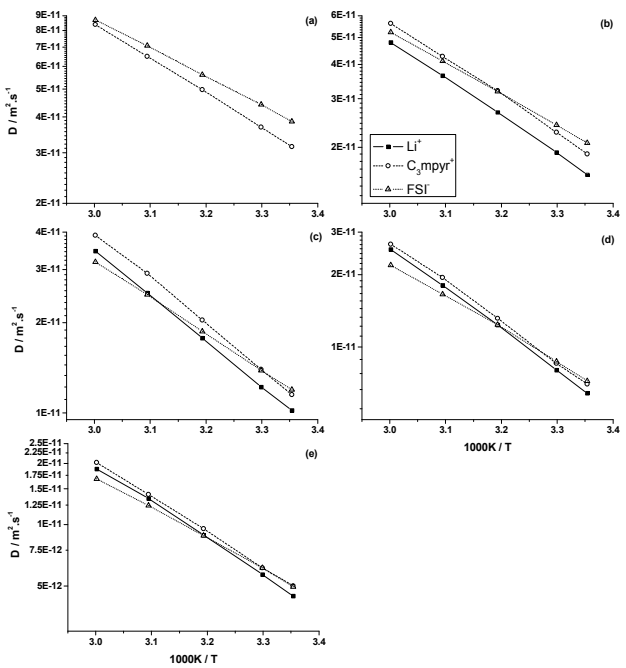

Figure 6 Diffusivities of Li^+, C_3mpyr and FSI ions measured using PFG-STE NMR from 25 °C to 60 °C. (a) neat C_3mpyrFSI; (b) 0.8 mol.kg^{-1}, (c) 1.6 mol.kg^{-1}, (d) 2.4 mol.kg^{-1}, and (e) 3.2 mol.kg^{-1} LiFSI in C_3mpyrFSI.

The diffusivity of each ion followed a simple Arrhenius equation:

$$D = D_0 \, exp(-\frac{E_A}{RT}), \qquad (5)$$

where, D is diffusivity at each temperature, D_0 is self diffusion constant, E_A is activation energy and R is the gas constant. The calculated D_0 and E_A values are presented in table 2. Both the self diffusion constants and activation energies of all ion species increased with increased Li salt concentration, hence the diffusivity decreased with increased salt concentration because of the increased activation energy, which is related to the strength of interaction between the ions.

Table 2 Parameters from Arrhenius fits to diffusivity data: self diffusion constant, D_0 and activation energy, E_A for each ion in C_3mpyrFSI ionic liquid as a function of LiFSI concentration. (< ±5%)

	Li^+		C_3mpyr		FSI	
	D_0 ($m^2.sec^{-1}$)	E_A ($kJ.mol^{-1}$)	D_0 ($m^2.sec^{-1}$)	E_A ($kJ.mol^{-1}$)	D_0 ($m^2.sec^{-1}$)	E_A ($kJ.mol^{-1}$)
Neat IL	-	-	$3.5e^{-7}$	23	$9.0e^{-8}$	19
0.8 mol.kg^{-1}	$5.9e^{-7}$	26	$6.2e^{-7}$	25	$1.4e^{-7}$	22
1.6 mol.kg^{-1}	$1.2e^{-6}$	29	$1.4e^{-6}$	29	$1.4e^{-7}$	23
2.4 mol.kg^{-1}	$3.2e^{-6}$	33	$2.8e^{-6}$	32	$2.7e^{-7}$	26
3.2 mol.kg^{-1}	$4.3e^{-6}$	34	$3.2e^{-6}$	33	$5.4e^{-7}$	29

According to Seki[44], who compared ILs containing imidazolium and phosphonium cations, a higher D_0 value results in lower viscosity and density, and higher ionic conductivity. However, in contrast to Seki's study with different ion species, our present system has the same cation and anion, and only differs in lithium concentration. In our case, the highest D_0 value occurs at the highest concentration, which is the sample with the highest viscosity and density and lowest ionic conductivity.

The diffusivity obtained by PFG-NMR does not distinguish between ion pairs and dissociated ions and is, rather, the average diffusivity over all possible species.[29] The NMR conductivity Λ_{NMR}, as calculated from the Nernst-Einstein equation (equation 3), assumes contributions from all individual ions, regardless of ion association. However, the molar conductivity obtained by impedance spectroscopy, Λ_{imp}, only includes conductivity due to dissociated ions or charged aggregates.[29] Hence, the ratio Λ_{imp} / Λ_{NMR} is referred to as the ionicity, and represents the degree of ion correlation within the IL; if the ionicity is unity, all ions are assumed to be dissociated and no ion pairs or ionic clusters are present.[29, 44-47] The calculated ionicity values for each solution are presented in table 3. The ionicity increases as temperature increases, but decreases with increased salt concentration; consistent with the previous interpretation of the diffusivity data. One interesting point here is that the ionicity was lowest when the Li salt concentration was 2.4 mol.kg^{-1} and increased again at 3.2 mol.kg^{-1}, after the addition of more Li salt. This also correlates with the Walden plot (shown previously in figure 4). This may indicate that the increased Li^+ concentration enhances the ion pair association or clustering for the neat IL to the 2.4 mol.kg^{-1} solutions but adding more Li^+ up to 3.2 mol.kg^{-1} does not contribute to ion pairing or clustering; instead the additional Li may exist as free Li^+ on the time scales of the measurements here.

Table 3 'Ionicity' of electrolytes indicating the degree of ion dissociation at each temperature and lithium salt concentration. (< ±5%)

Λ_{Imp} / Λ_{NMR}	25 °C	30 °C	40 °C	50 °C	60 °C
Neat IL	0.56	0.57	0.57	0.58	0.58
0.8 mol.kg^{-1}	0.50	0.51	0.51	0.53	0.53
1.6 mol.kg^{-1}	0.46	0.48	0.49	0.50	0.50
2.4	0.35	0.36	0.37	0.39	0.40

mol.kg^{-1}					
3.2 mol.kg^{-1}	0.39	0.40	0.42	0.43	0.43

We have calculated using Nernst-Einstein equation (eq. 3) the Li^+ partial conductivity from the NMR diffusivity data presented in figure 6 and the result is shown in figure 7. While the actual total conductivity decreases (figure 2(a) and (b)) with increased salt concentration, the Li^+ partial conductivity increases up to 1.6 mol.kg^{-1} the contributions of the C_3mpyr and FSI conductivities decrease as the relative molar fraction of Li^+ increases.

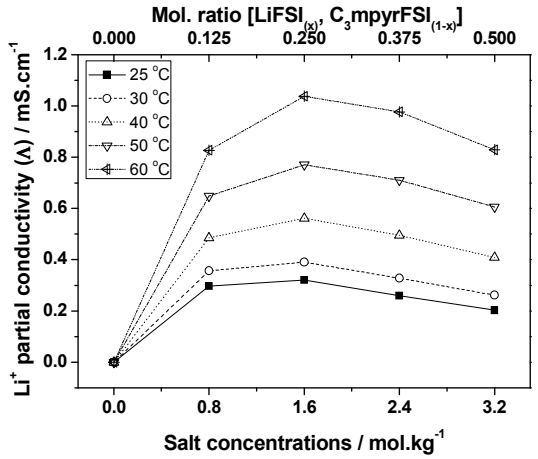

Figure 7 The partial conductivity of Li^+ in the solution, calculated from the ionic mobility data.

A reciprocal viscosity vs. lithium diffusion coefficient plot to check Li^+ solvation number using Stoke-Einstein relationship is demonstrated in supplementary figure 4. It is shown that the effective radii of Li^+ is not changing with temperature.

FSI configuration with Li salts:

In order to rationalise the increased partial Li^+ conductivity and the phenomena observed in the ionicity plot, we have used FT-IR and Raman spectroscopy to study the interactions between Li^+, C_3mpyr, and FSI. The FT-IR and Raman spectra for each Li salt concentration are presented in figure 8. We have assigned the peaks based on the assignments for 0.5 mol.kg^{-1} LiTFSI in C_3mpyrFSI by Hardwick et al.[48]

Figure 8 (a) presents the FT-IR spectra for various LiFSI concentrations in the C_3mpyrFSI. The S-N-S stretching peaks at 730 and 830 cm^{-1} respectively, become restricted and shift to higher wavenumber, with S-F asymmetrical stretching (830 cm^{-1}) closer to the peak position in the pure LiFSI salt. These changes are anticipated as both symmetric and asymmetric bond stretching in FSI will be strongly associated with the Li ion.

Figure 8 (b) shows the FT-IR spectra for the asymmetric SO_2 bending that is located at 564 cm^{-1}. A shoulder appears at ~595 cm^{-1} which increases in intensity with increasing salt concentration, a phenomena was has also been reported by Huang et al.[27] Raman peaks in figure 8 (c) and 8 (d) were assigned according to the previous reports by Fujii et al.[18] and Castriota et al.[49]. The data show that the peaks at 1215 cm^{-1} ($\upsilon(SO_2)$) and 720 cm^{-1} (υ_S(SNS)) are shifted toward higher frequency and peak broadening occurs as the LiFSI salt concentration increases. Together, these three spectra imply there are changes in the coordination between FSI and Li^+ which we ascribe to ion-paring effects in the electrolyte. Due to the high salt concentrations, and the peaks in the spectra being quite broad in nature, we would also expect that there are higher levels of ion-pairing present such as doubles, triples and polymer-like aggregates. This observation is consistent with the ionicity data presented earlier. Hardwick et al. also reported that the Raman peaks shift to higher frequency for the TFSI system (figure 8 (c)) which indicates that Li^+ is bound to the TFSI anion[50]; this interpretation is consistent with our observations in the FSI system studied here.

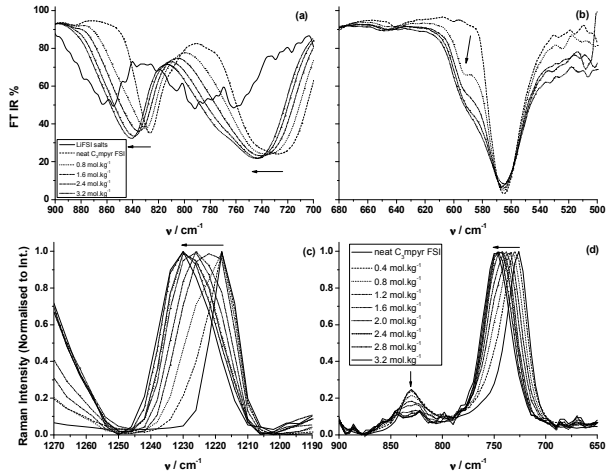

Figure 8 FT-IR transmittance and Raman spectra; (a) FT-IR from 900 to 700 cm^{-1}, (b) FT-IR from 680 to 500 cm^{-1}, (c) Raman from 1270 to 1190 cm^{-1}, (d) Raman from 900 to 650 cm^{-1}. Note that the intensities of the LiFSI salt spectra in FT-IR (a) (thin black) were magnified. (This figure, resolution, etc..)

Furthermore, Fujii et al. calculated theoretical Raman peak positions and compared them with experimental Raman spectra.[24, 25] The peaks for the trans-form of FSI (or C2 conformer) were calculated in the liquid phase to be at 353, 316 and 275 cm^{-1} and the peaks for a cis-form (or C1 conformer) were calculated as 344, 315 and 278 cm^{-1}. While the absolute peak positions in this experiment are slightly different from these calculated values, we speculate that Figure 9 may show that the trans-form of the FSI conformer is changing into the cis-form with increasing Li^+ concentration.

The FT-IR and Raman spectra show that a percentage of FSI anions are converted from the trans- to cis- conformer as increasing amounts of Li salt is added to the IL. Fujii et al. have shown, using Raman and ab-initio calculations, that the binding energy of Li^+ in the cis- conformer is lower than in the trans-conformer.[51] Such a change may allow Li ions to move via a site activation model, analogous to that observed in polymer electrolytes. Furthermore, their recent research[52] revealed that

unlike the $[Li(NTf_2)_2]^-$ complex formed in NTf_2 (or TFSI), $[Li(FSI)_3]^{2-}$ complex is preferentially formed in FSI-based ILs in the dilute region less than 1 mol.kg^{-1}.[52] Depletion of the FSI anion at the higher concentrations shown in this research (i.e. Li : FSI ratio approaching 2) may indicate formation of a smaller cluster (e.g. $Li(FSI)_2$) which would result in different Li^+ transport behavior to that observed in Fujii's study. This would be consistent with the increase in population of the cis-form of FSI with increasing Li^+ concentration. One could therefore postulate that these changes may affect the transport mechanism of Li^+ at these high salt concentrations, going from a 1:3 to 1:2 Li^+:FSI speciation, but also from a vehicular transport dominated mechanism to a mixed conduction mechanism in these viscous systems.

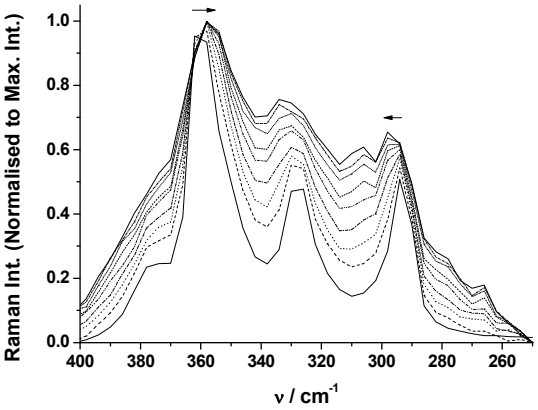

Figure 9 Selected regions of Raman spectra in 400 – 250 cm^{-1} range. Note that all peaks were baseline corrected and normalized to the maximum intensity or area. Arrow indicates direction of increasing LiFSI concentration.

Conclusions

We have previously shown that high concentration FSI based ionic liquid electrolytes display interesting electrochemical properties, exhibit high Li^+ transport number and excellent rate capability in lithium batteries. This work seeks to understand why this might be the case through the use of a number of different physical characterisation techniques. The conductivity, viscosity, density and DSC data for C_3mpyrFSI with different LiFSI salt concentrations from 0 to 3.2 mol.kg^{-1} (1 : 1: 2 molar ratio of Li^+ : C_3mpyr : FSI) are reported. The Walden plots and ionicity data show that these electrolytes exhibit behaviour closer to that of an ideal IL at the higher salt concentration of 3.2 mol.kg^{-1} (or 0.5 mol fraction). FT-IR and Raman spectra show two distinct behaviours; ion-paring with increasing salt concentration and a shift in the preferred conformation of the anion to a mixture of cis- / trans- FSI species. As the lithium concentration increases, the conformation of FSI changes from largely trans- to a mostly cis- form. The changes in the local structure of the FSI based electrolytes leads us to postulate that this may be the origin of the enhanced transport properties.

^{7}Li NMR showed a shift to higher fields, consistent with a more electron-shielded environment as the Li^+ concentration increased. The NMR diffusivity measurements show that, at a high lithium concentration, the mobility of Li^+ relative to that of the other ionic species is greater than in solutions with lower lithium concentrations. These results may imply that the coordination of the lithium ion in the FSI based IL containing a high Li^+ concentration is different, and that the Li^+ transport mechanism may be different from that seen in TFSI based ILs or FSI based ILs at low Li salt concentrations.

Acknowledgements

We thank the ARC (Australian Research Council) and CSIRO's Energy Transformed National Research Flagship for funding this research. The authors would also like to thank Dr. Tony Hollenkamp (CSIRO) for fruitful discussions on this manuscript. MF and DRM are grateful to the Australian Research Council for support under the Australian Laureate Fellowship scheme.

Notes and references

[a] ARC Centre of Excellence for Electromaterials Science (ACES), Institute for Frontier Materials (IFM), Deakin University, Burwood, Victoria 3125, Australia. E-mail: hyun.yoon@deakin.edu.au

[b] Commonwealth Scientific and Industrial Research Organisation (CSIRO), Division of Energy Technology, Bayview Ave., Clayton, 3169 Victoria, Australia

[c] School of Chemistry, Monash University, 3800 Victoria, Australia

Electronic Supplementary Information (ESI) available: [details of any supplementary information available should be included here]. See DOI: 10.1039/b000000x/

1. J. H. Shin, W. A. Henderson and S. Passerini, *Electrochem. Commun.*, 2003, **5**, 1016-1020.
2. H. Matsumoto, H. Sakaebe, K. Tatsumi, M. Kikuta, E. Ishiko and M. Kono, *J. Power Sources*, 2006, **160**, 1308-1313.
3. , EP850920-A; WO9829358-A; etc.
4. K. Zaghib, P. Charest, A. Guerfi, J. Shim, M. Perrier and K. Striebel, *J. Power Sources*, 2004, **134**, 124-129.
5. M. Ishikawa, T. Sugimoto, M. Kikuta, E. Ishiko and M. Kono, *J. Power Sources*, 2006, **162**, 658-662.
6. A. Guerfi, S. Duchesne, Y. Kobayashi, A. Vijh and K. Zaghib, *J. Power Sources*, 2008, **175**, 866-873.
7. J. Saint, A. S. Best, A. F. Hollenkamp, J. Kerr, J. H. Shin and M. M. Doeff, *J. Electrochem. Soc.*, 2008, **155**, A172-A180.
8. S. Seki, Y. Kobayashi, H. Miyashiro, Y. Ohno, Y. Mita, N. Terada, P. Charest, A. Guerfi and K. Zaghib, *J. Phys. Chem. C*, 2008, **112**, 16708-16713.
9. Q. Zhou, W. A. Henderson, G. B. Appetecchi, M. Montanino and S. Passerini, *J. Phys. Chem. B*, 2008, **112**, 13577-13580.
10. E. Paillard, Q. Zhou, W. A. Henderson, G. B. Appetecchi, M. Montanino and S. Passerini, *J. Electrochem. Soc.*, 2009, **156**, A891-A895.
11. A. S. Best, A. I. Bhatt and A. F. Hollenkamp, *J. Electrochem. Soc.*, 2010, **157**, A903-A911.
12. A. I. Bhatt, A. S. Best, J. Huang and A. F. Hollenkamp, *J. Electrochem. Soc.*, 2010, **157**, A66-A74.
13. A. Lewandowski and I. Acznik, *Electrochim. Acta*, 2010, **56**, 211-214.
14. Y. Wang, K. Zaghib, A. Guerfi, F. F. C. Bazito, R. M. Torresi and J. R. Dahn, *Electrochim. Acta*, 2007, **52**, 6346-6352.
15. A. Abouimrane, J. Ding and I. J. Davidson, *J. Power Sources*, 2009, **189**, 693-696.

16. R. Vijayaraghavan, M. Surianarayanan, V. Armel, D. R. MacFarlane and V. P. Sridhar, *Chem. Commun.*, 2009, 6297-6299.
17. P. Johansson, S. P. Gejji, J. Tegenfeldt and J. Lindgren, *Electrochim. Acta*, 1998, **43**, 1375-1379.
18. K. Fujii, T. Fujimori, T. Takamuku, R. Kanzaki, Y. Umebayashi and S. I. Ishiguro, *Journal of Physical Chemistry B*, 2006, **110**, 8179-8183.
19. Y. Umebayashi, T. Mitsugi, S. Fukuda, T. Fujimori, K. Fujii, R. Kanzaki, M. Takeuchi and S.-I. Ishiguro, *Journal of Physical Chemistry B*, 2007, **111**, 13028-13032.
20. A. Shirai, K. Fuji, S. Seki, Y. Umebayashi, S.-i. Ishiguro and Y. Ikeda, *Anal. Sci.*, 2008, **24**, 1291-1296.
21. S.-i. Ishiguro, Y. Umebayashi, R. Kanzaki and K. Fujii, *Pure and Applied Chemistry*, 2010, **82**, 1927-1941.
22. Y. Umebayashi, T. Yamaguchi, S. Fukuda, T. Mitsugi, M. Takeuchi, K. Fujii and S.-i. Ishiguro, *Anal. Sci.*, 2008, **24**, 1297-1304.
23. M. Beran, J. Prihoda, Z. Zak and M. Cernik, *Polyhedron*, 2006, **25**, 1292-1298.
24. K. Fujii, S. Seki, S. Fukuda, R. Kanzaki, T. Takamuku, Y. Ulmebayashi and S.-i. Ishiguro, *J. Phys. Chem. B*, 2007, **111**, 12829-12833.
25. K. Fujii, S. Seki, S. Fukuda, T. Takamuku, S. Kohara, Y. Kameda, Y. Umebayashi and S. Ishiguro, *J. Mol. Liq.*, 2008, **143**, 64-69.
26. J. N. C. Lopes, K. Shimizu, A. A. H. Padua, Y. Umebayashi, S. Fukuda, K. Fujii and S.-i. Ishiguro, *J. Phys. Chem. B*, 2008, **112**, 9449-9455.
27. J. Huang and A. F. Hollenkamp, *J. Phys. Chem. C*, 2010, **114**, 21840-21847.
28. H. Yoon, P. C. Howlett, A. S. Best, M. Forsyth and D. R. MacFarlane, *Journal of the Electrochemical Society*, 2013, **160**, A1629-A1637.
29. P. M. Bayley, G. H. Lane, N. M. Rocher, B. R. Clare, A. S. Best, D. R. MacFarlane and M. Forsyth, *Phys. Chem. Chem. Phys.*, 2009, **11**, 7202-7208.
30. A. Guerfi, M. Dontigny, Y. Kobayashi, A. Vijh and K. Zaghib, *J. Solid State Electrochem.*, 2009, **13**, 1003-1014.
31. K. Hayamizu, S. Tsuzuki, S. Seki, K. Fujii, M. Suenaga and Y. Umebayashi, *J. Chem. Phys.*, 2010, **133**.
32. P. Johansson, L. E. Fast, A. Matic, G. B. Appetecchi and S. Passerini, *J. Power Sources*, 2010, **195**, 2074-2076.
33. M. Kunze, M. Montanino, G. B. Appetecchi, S. Jeong, M. Schoenhoff, M. Winter and S. Passerini, *J. Phys. Chem. A*, 2010, **114**, 1776-1782.
34. M. Kunze, S. Jeong, E. Paillard, M. Winter and S. Passerini, *J. Phys. Chem. C*, 2010, **114**, 12364-12369.
35. C. A. Angell, N. Byrne and J.-P. Belieres, *Accounts Chem. Res.*, 2007, **40**, 1228-1236.
36. W. Xu, E. I. Cooper and C. A. Angell, *J. Phys. Chem. B*, 2003, **107**, 6170-6178.
37. S. Ferrari, E. Quartarone, P. Mustarelli, A. Magistris, S. Protti, S. Lazzaroni, M. Fagnoni and A. Albini, *J. Power Sources*, 2009, **194**, 45-50.
38. K. Ueno, H. Tokuda and M. Watanabe, *Phys. Chem. Chem. Phys.*, 2010, **12**, 1649-1658.
39. T. Makino, M. Kanakubo, T. Umecky, A. Suzuki, T. Nishida and J. Takano, *Journal of Chemical and Engineering Data*, 2012, **57**, 751-755.
40. D. R. MacFarlane, M. Forsyth, E. I. Izgorodina, A. P. Abbott, G. Annat and K. Fraser, *Phys. Chem. Chem. Phys.*, 2009, **11**, 4962-4967.
41. K. J. Fraser, E. I. Izgorodina, M. Forsyth, J. L. Scott and D. R. MacFarlane, *Chem. Commun.*, 2007, 3817-3819.
42. T. Takamuku, Y. Kyoshoin, T. Shimomura, S. Kittaka and T. Yamaguchi, *Journal of Physical Chemistry B*, 2009, **113**, 10817-10824.
43. K. Matsumoto, R. Hagiwara and O. Tamada, *Solid State Sci.*, 2006, **8**, 1103-1107.
44. S. Seki, K. Hayamizu, S. Tsuzuki, K. Fujii, Y. Umebayashi, T. Mitsugi, T. Kobayashi, Y. Ohno, Y. Kobayashi, Y. Mita, H. Miyashiro and S.-i. Ishiguro, *Phys. Chem. Chem. Phys.*, 2009, **11**, 3509-3514.
45. H. Tokuda, K. Hayamizu, K. Ishii, M. Abu Bin Hasan Susan and M. Watanabe, *J. Phys. Chem. B*, 2004, **108**, 16593-16600.
46. H. Tokuda, S. Tsuzuki, M. Susan, K. Hayamizu and M. Watanabe, *J. Phys. Chem. B*, 2006, **110**, 19593-19600.
47. A. Fernicola, B. Scrosati and H. Ohno, *Ionics*, 2006, **12**, 95-102.
48. L. J. Hardwick, J. A. Saint, I. T. Lucas, M. M. Doeff and R. Kostecki, *J. Electrochem. Soc.*, 2009, **156**, A120-A127.
49. M. Castriota, T. Caruso, R. G. Agostino, E. Cazzanelli, W. A. Henderson and S. Passerini, *J. Phys. Chem. A*, 2005, **109**, 92-96.
50. L. J. Hardwick, M. Hahn, P. Ruch, M. Holzapfel, W. Scheifele, H. Buqa, F. Krumeich, P. Novak and R. Koetz, *Electrochim. Acta*, 2006, **52**, 675-680.
51. K. Fujii, T. Nonaka, Y. Akimoto, Y. Umebayashi and S.-i. Ishiguro, *Anal. Sci.*, 2008, **24**, 1377-1380.
52. K. Fujii, H. Hamano, H. Doi, X. Song, S. Tsuzuki, K. Hayamizu, S. Seki, Y. Kameda, K. Dokko, M. Watanabe and Y. Umebayashi, *J. Phys. Chem. C*, 2013, **117**, 19314-19324.

